Jet-installation noise reduction with flow-permeable materials

Journal of Sound and Vibration 498 (2021) 115959

Contents lists available at ScienceDirect

Journal of Sound and Vibration

journal homepage: www.elsevier.com/locate/jsv

Jet-installation noise reduction with flow-permeable materials

Leandro Rego[a,*], Daniele Ragni[a], Francesco Avallone[a], Damiano Casalino[a], Riccardo Zamponi[b], Christophe Schram[b]

[a] Delft University of Technology, Department of Aerodynamics, Wind Energy and Propulsion, Kluyverweg 1, 2629 HS, Delft, the Netherlands

[b] von Kármán Institute for Fluid Dynamics, Environmental & Applied Fluid Dynamics Department, Waterloosesteenweg 72, Sint-Genesius-Rode 1640, Belgium

ARTICLE INFO

Article history:
Received 16 October 2019
Revised 31 August 2020
Accepted 16 January 2021
Available online 22 January 2021

Keywords:
Aeroacoustics
Jet-installation noise
Porous materials

ABSTRACT

This paper investigates the application of flow-permeable materials as a solution for reducing jet-installation noise. Experiments are carried out with a flat plate placed in the near field of a single-stream subsonic jet. The flat plate is modular and the solid surface near the trailing edge can be replaced with different flow-permeable inserts, such as a metal foam and a perforated plate structure. The time-averaged jet flow field is characterized through planar PIV measurements at three different velocities ($M_a = 0.3$, $M_a = 0.5$ and $M_a = 0.8$, where M_a is the acoustic Mach number), whereas the acoustic far-field is measured with a microphone arc-array. Acoustic measurements confirm that installation effects cause significant noise increase, up to 17 dB for the lowest jet velocity, particularly at low and mid frequencies (i.e. $St < 0.7$, with the Strouhal number based on the jet diameter and velocity), and mostly in the upstream direction of the jet. By replacing the solid trailing edge with the metal foam, noise abatement of up to 9 dB is achieved at the spectral peak for $M_a = 0.3$ and a polar angle $\theta = 40^\circ$, with an overall reduction in the entire frequency range where jet-installation noise is dominant. The perforated plate provides lower noise reduction than the metal foam (7 dB at the spectral peak for $M_a = 0.3$ and $\theta = 40^\circ$), and it is less effective at low frequencies. This is related to the values of permeability and form coefficient of the materials, which are the major parameters controlling the pressure balance across the trailing edge and, consequently, the noise generated by the plate. However, despite having a high permeability, the plate with the metal-foam trailing edge still has a distinct noise production at mid frequencies ($St \approx 0.43$ for $M_a = 0.3$). Based on the analyses of different treated surface lengths, it is conjectured that the solid-permeable junction in the plate acts as a new scattering region, and thus its position also affects the far-field noise, which is in line with analytical predictions in the literature. Nonetheless, both types of inserts provide significant noise reduction and are potential solutions for the problem of jet-installation noise.

* Corresponding author.
E-mail address: l.rego@tudelft.nl (L. Rego).

https://doi.org/10.1016/j.jsv.2021.115959

1. Introduction

Jet-installation noise (JIN) arises from the interaction between the exhaust flow of an aircraft jet engine and a nearby airframe surface [1,2]. It has been shown that the presence of solid boundaries in the vicinity of a jet flow highly affects the acoustic characteristics of the system. For the case of an installed subsonic jet, aside from the turbulence-mixing noise component, there is an additional source at the surface trailing edge [3]. This region acts as a singularity for convecting hydrodynamic pressure waves, which are generated by the jet mixing-layer, resulting in their scattering as noise. This phenomenon is responsible for noise increase at low and mid frequencies, particularly in the directions normal and upstream of the jet axis, equivalent to a distribution of acoustic dipoles at the trailing edge [4–6]. Installation effects are also responsible for reflection of acoustic waves generated by quadrupole sources in the jet plume [7]. Recent computational results of aircraft acoustic footprint have shown that installation effects are responsible for penalties of approximately 4 EPNdB at full aircraft level [8]. In the near future, with the development of ultra-high bypass ratio engines, this source will likely become more dominant due to increased proximity between engine and airframe [9]. Therefore, the development of noise reduction solutions for this particular source is of interest.

Attempts to reduce JIN were performed by Mengle et al. [10] through the use of chevron nozzles. Wind tunnel tests of a jet-flap configuration with different nozzle geometries were carried out. The results, obtained from beamforming applied to phased-array microphone measurements, showed that the chevrons reduced noise up to 2.6 dB at the spectral peak [10]. However, although the chevrons provided some benefits, they were still not sufficient to bring the noise of the configuration back to isolated jet levels, and thus the trailing-edge source was still present.

A possible solution for JIN reduction is the application of porous materials on the scattering surface. Similar concepts have been investigated, but for different applications. Revell et al. [11] reported flap side-edge noise mitigation when the surface was treated with porous materials. It was conjectured that the reductions in surface pressure fluctuations and far-field sound were attributed to dissipation of acoustic waves, flow communication between upper and lower side (reducing the pressure imbalance between them), and lower impedance of the surface interacting with the vortex [11]. Experiments performed by Sarradj and Geyer [12] showed that a fully porous SD7003 airfoil reduces turbulent boundary-layer trailing-edge (TBL-TE) noise up to 10 dB compared to the solid case. The properties of the material, such as porosity and resistivity, were found to affect the frequency range and amplitude of noise reduction [12]. However, such reduction was coupled with a significant loss in performance (lift decrease and drag increase). In order to mitigate these negative effects, the authors restricted the porous section of the airfoil to the trailing-edge region [13]. The shortest porous length (last 5% of the airfoil chord) provided 8 dB noise reduction with minor effects on the aerodynamic characteristics.

Herr et al. [14] investigated TBL-TE noise reduction on a DLRF16 airfoil by applying porous materials on the last 10% of the chord. Results showed significant noise reduction at low frequencies with respect to the solid case. Another important conclusion was that communication between the pressure and suction sides of the airfoil was necessary to obtain noise reduction [14], indicating that an improvement of the pressure balance is essential. More recently, Rubio-Carpio et al. [15,16] studied the reduction of TBL-TE noise by replacing sections of the trailing edge (last 20% of the chord) with porous inserts manufactured out of metallic foams. Acoustic beamforming results showed noise reduction at low and mid frequencies, on the order of 10 dB with respect to the solid airfoil, and an increase at high frequencies, which was attributed to the surface roughness of the porous material. Possible explanations for the noise reduction were related to changes in the turbulence intensity and Reynolds stresses in the boundary-layer, as well as a different radiation efficiency at the edge (reduction in the acoustic impedance discontinuity at the trailing edge) [16].

Despite the positive results achieved for airfoil TBL-TE and flap side-edge noise, there has been no attempt yet to apply this technology for JIN reduction. It is conjectured that the pressure imbalance on a surface in the vicinity of a jet, caused by impinging waves on only one side, can be alleviated through the application of flow-permeable materials. This effect, coupled with a less abrupt jump in impedance at the trailing-edge region, is likely to result in noise abatement. Therefore, this work aims to investigate the capability of flow-permeable materials to provide noise reduction for an installed jet by mitigating the trailing-edge source, and achieving sound levels close to those of an isolated jet. For this purpose, experiments are carried out with a flat plate placed in the vicinity of a single-stream subsonic jet. The trailing edge of the plate can be replaced with a metal foam insert, similarly as performed by Rubio-Carpio et al. [15], or a perforated flow-permeable structure with straight holes orthogonal to the jet axis. Particle Image Velocimetry (PIV) is used to characterize the jet flow field in terms of time-averaged and root-mean-square (r.m.s.) velocity. Acoustic measurements are also performed with microphones mounted in an arc-array. Far-field spectra of isolated and installed jets (solid plate) are compared to the installed cases with flow-permeable trailing edges. The influence of the jet velocity and the geometry of the configuration is also addressed.

This paper is organized as follows. In Section 2, the experimental set-up is described, including the characteristics of the flow-permeable materials. In Section 3, the results of the experiments are discussed. The jet flow field characterization is reported through PIV measurements. Acoustic results of the isolated and installed configurations are also included, along with the effects of flow-permeable materials on installation noise. Finally, the conclusions of this work are summarized in Section 4.

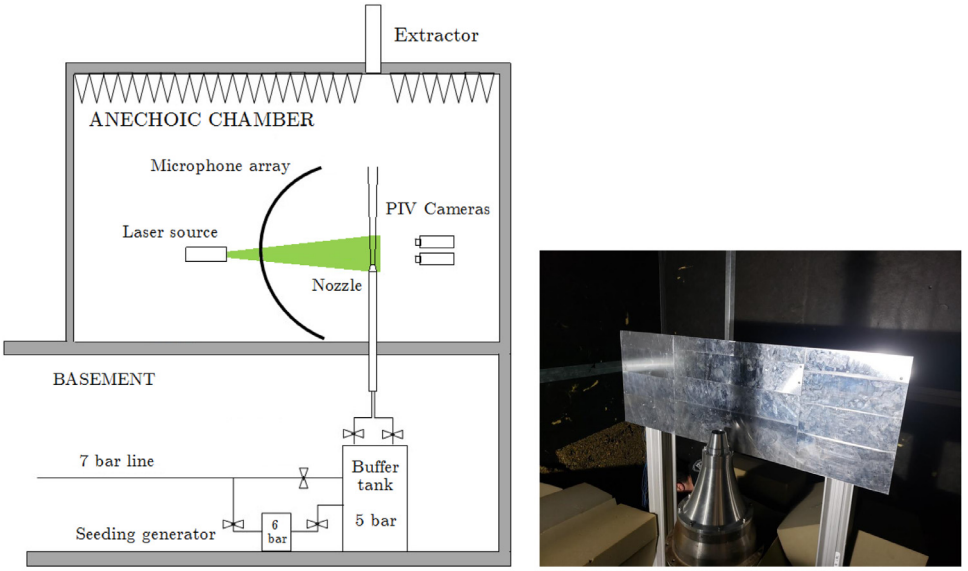

Fig. 1. (a) Sketch of the FAST facility layout with a nozzle mounted in the anechoic chamber and the air supply system at the basement below. Adapted from [17]. (b) Nozzle mounted with the flat plate inside the facility.

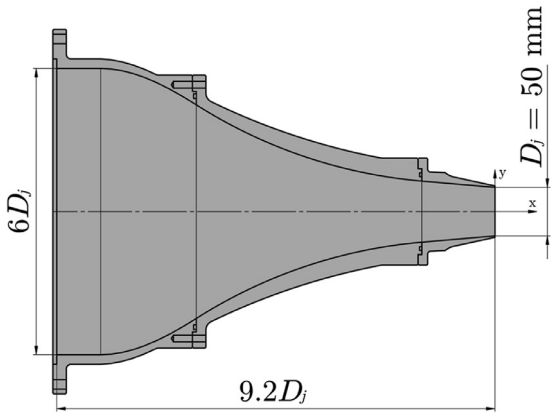

Fig. 2. Cut view of the nozzle (dimensions as function of the exit diameter $D_j = 50$ mm).

2. Experimental set-up

2.1. Facility and models

The experiments are performed in the Free jet AeroacouSTic facility (FAST) at the von Kármán Institute for Fluid Dynamics (VKI). This facility consists of a circular jet rig placed in a semi-anechoic room, as shown in Fig. 1a, with a cut-off frequency of 350 Hz [17]. For the tests performed in this work, the air is supplied by a 7 bar pressure line located beneath the test chamber. The line is also bypassed to a seeding generator for PIV measurements. The seeded flow merges with the pressurized air in a buffer tank to ensure correct mixing. The jet blows vertically into an extractor equipped with a muffler [17]. In the anechoic chamber, a laser source and cameras are mounted for PIV measurements, whereas a microphone arc-array is present for the acoustic ones. The picture in Fig. 1b shows the jet nozzle installed with the flat plate inside the facility.

A circular convergent nozzle with an exit diameter $D_j = 50$ mm and contraction ratio of 36:1 is designed based on the geometry of the SMC000 nozzle, which has been used for several investigations of isolated and installed subsonic turbulent jets [2,18,19]. This nozzle, manufactured in aluminium, is attached to a straight pipe with 300 mm of diameter. A cut view of the nozzle is shown in Fig. 2 along with its main dimensions. The origin of the coordinates system used in the analyses is positioned at the center of the nozzle exit plane.

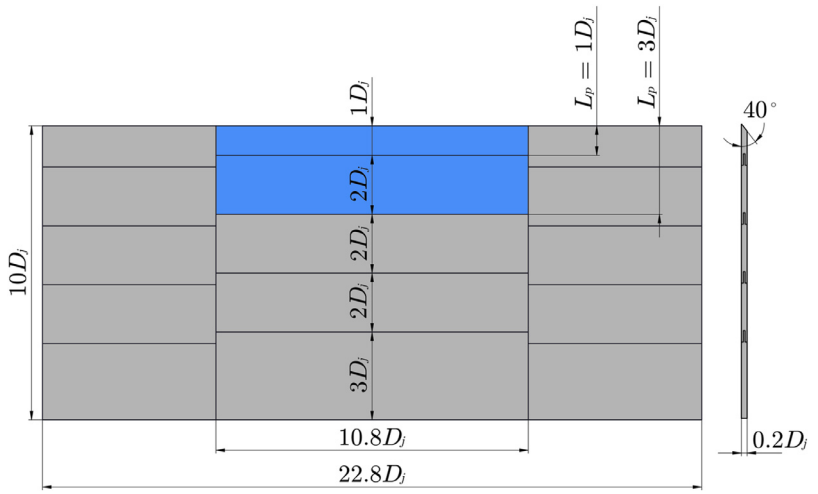

Fig. 3. Modular flat plate (dimensions as function of the exit diameter D_j). Pieces shown in blue can be replaced by the flow-permeable materials. (For interpretation of the references to color in this figure legend, the reader is referred to the web version of this article.)

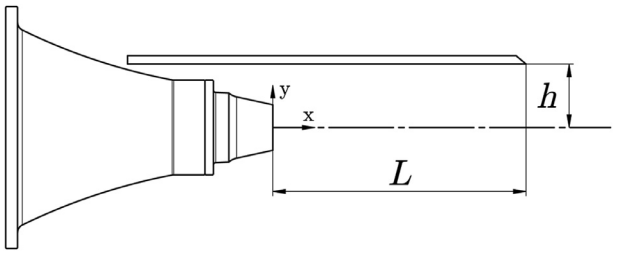

Fig. 4. Installed jet configuration. Geometric cases are investigated by changing the flat plate length L and radial position h.

Table 1
Jet flow conditions in terms of acoustic Mach number (M_a), nozzle pressure ratio (NPR), temperature ratio (T_R) and Reynolds number (Re).

Condition	M_a [-]	NPR [-]	T_R [-]	Re [10^5]
1	0.3	1.06	0.988	3.58
2	0.5	1.18	0.959	6.16
3	0.8	1.54	0.892	10.6

For the installed configuration, a stainless steel flat plate is mounted in the vicinity of the nozzle. The plate is realized with a modular structure, which allows for different surface lengths to be easily investigated. The length of each part is shown in Fig. 3. The surface has a total dimension of 500 mm × 1140 mm × 10 mm. The large width is chosen to avoid side-edge scattering. The aft piece consists of a sharp trailing edge with a chamfer angle of 40°. This modular design also allows for an easy replacement of the solid structure by the flow-permeable materials. Two pieces at the middle section (shown in blue in Fig. 3) can be replaced by the flow-permeable ones, allowing for the investigation of different porosity lengths ($L_p = 1D_j$ and $L_p = 3D_j$).

Different geometric cases are tested by changing the length L and height h of the plate. As shown in Fig. 4, the length is defined as the distance between the trailing edge and the nozzle exit plane, and the height as the radial position with respect to the jet centerline. A baseline installed case is defined with $L = 6D_j$ and $h = 1.5D_j$. The leading edge of the plate is mounted upstream of the nozzle exit plane to avoid scattering at that region. A different plate length is also investigated ($L = 8D_j$) for a fixed $h = 1.5D_j$, as well as a different radial position ($h = 2D_j$) for a fixed $L = 6D_j$. Due to set-up constraints, it is not possible to mount the plate at a radial position $h < 1.5D_j$. Therefore, the effect of the plate height is addressed by moving it away from the jet. Moreover, with a length shorter than $L = 6D_j$ at that position, it is possible that the relative noise increase due to installation effects would be much lower, particularly for mid and high jet Mach numbers, which could compromise the parametric analysis of the flow-permeable treatment.

The tests are performed at three jet flow velocities with different acoustic Mach numbers M_a, where the jet velocity U_j is divided by the ambient speed of sound c_0. The flow characteristics such as the nozzle pressure ratio (NPR) and the static temperature ratio T_R are reported in Table 1, as well as the Reynolds number Re, based on the nozzle exit diameter. The

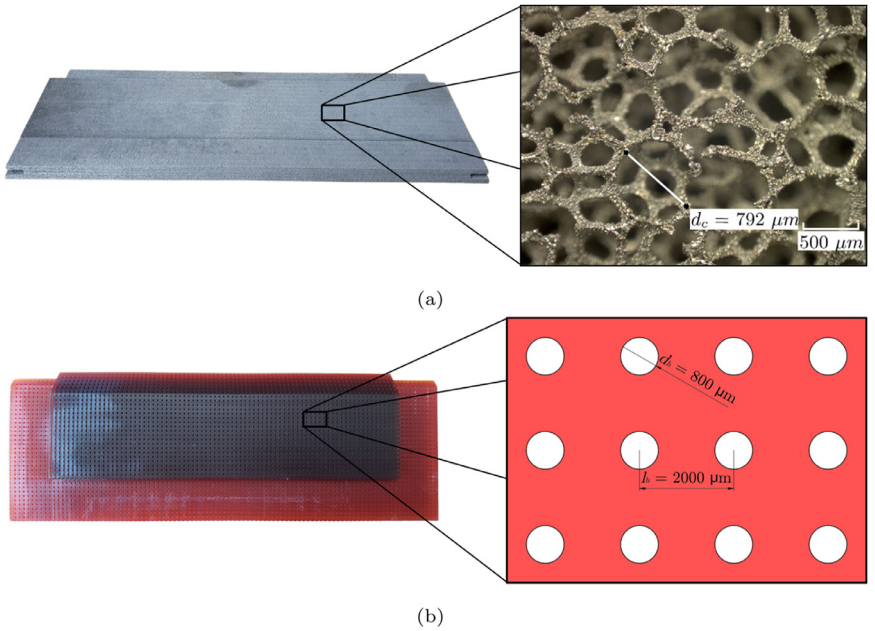

Fig. 5. Flow-permeable trailing-edge inserts applied to the flat plate. (a) Metal foam - $d_c = 800$ µm. Adapted from [16]. (b) Perforated - $d_h = 800$ µm. Dimensions in µm.

measurements are conducted at static conditions, i.e. no flow external to jet, at average ambient conditions of $p_{\text{amb}} = 100.6$ kPa and $T_{\text{amb}} = 294$ K.

2.2. Flow-permeable materials

Two types of noise reduction solutions based on flow-permeable materials are investigated in this work. The first one is an open-cell NiCrAl foam manufactured by the company Alantum. The metal foam is manufactured through electrodeposition of pure Ni on a polyurethane foam, which is subsequently coated with high-alloyed powder [20]. This type of material consists of a homogeneous microstructure with a three-dimensional repetition of a dodecahedron-shaped cell [16]. Rubio-Carpio et al. [15] have investigated the application of this material with different cell diameters d_c for airfoil TBL-TE noise reduction. A structure with nominal $d_c = 800$ µm is chosen for this work since its porosity and permeability characteristics are available, and significant TBL-TE noise reduction was obtained with this structure [15]. Two inserts are manufactured for the plate, as shown in Fig. 5a in order to assess the effect of porosity length on the noise reduction. The second type of flow-permeable material consists of a 3D-printed perforated insert with straight holes connecting the upper and lower side of the plate, as shown in Fig. 5b. This insert is manufactured in R5, which is a liquid photopolymer that offers good surface finishing and strength properties [21]. The holes have a diameter $d_h = 800$ µm and a spacing of $l_h = 2$ mm.

The flow-permeable materials are characterized by properties such as porosity σ and permeability K. The porosity is defined as the ratio between the volumetric densities of the flow-permeable material ρ_p and of the solid structure ρ_s, as shown in Eq. (1):

$$\sigma = 1 - \frac{\rho_p}{\rho_s}. \tag{1}$$

The permeability is obtained through the Hazen-Dupuit-Darcy equation (Eq. (2)), which prescribes the static pressure loss Δp across a homogeneous sample with thickness t [22]:

$$\frac{\Delta p}{t} = \frac{\mu}{K} v_d + \rho C v_d^2, \tag{2}$$

where μ is the flow dynamic viscosity, ρ is the flow density, v_d is the Darcian velocity (defined as the ratio between the volumetric flow rate and the cross-section area of the sample [22]), and K and C are the permeability and form coefficients, which account for pressure losses due to viscous and inertial effects, respectively.

For the metal foam, the porosity and permeability parameters were obtained by Rubio-Carpio et al. [15]. The former was obtained by measuring the density of small samples, whereas the latter was obtained from characterization experiments performed with a permeability rig [15]. The results are reported in Table 2. A similar procedure has been carried out for the 3D-printed perforated material. The resistivity R ($R = \mu/K$) is also included in the table for comparison.

Table 2
Properties of the flow-permeable materials in terms of cell diameter (d_c), porosity (σ), permeability (K), and resistivity (R) and form coefficient (C).

Material	d_c [μm]	σ [%]	K [$\times 10^{-9}$ m^2]	R [Ns/m^4]	C [m^{-1}]
Metal foam	0.8	91.7	2.71	6728	2612
Perforated	0.8	12.6	1.58	11540	7283

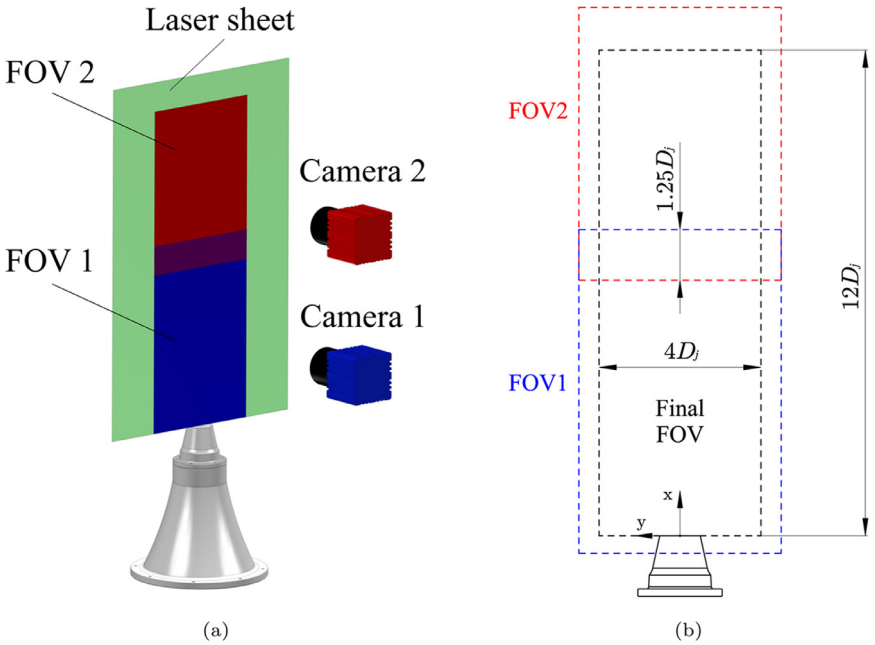

Fig. 6. (a) Concept of the PIV set-up with 2 cameras and 2 fields-of-view. (b) Fields-of-view from each camera (blue and red planes) and final FOV (black), with dimensions. (For interpretation of the references to color in this figure legend, the reader is referred to the web version of this article.)

2.3. Instrumentation and measurement techniques

2.3.1. Flow field measurements

A two-dimensional jet velocity field is obtained through PIV measurements on the *xy*-plane (normal to the nozzle exit). This method allows for the measurements of time-averaged velocity components u and v (in the axial and radial directions, respectively), and the r.m.s. of their fluctuations u'_{rms} and v'_{rms}. The PIV measurements are performed only for the isolated jet configuration, since the investigated configurations (length and height) are chosen such to avoid grazing flow on the surface. It has been shown in a previous investigation that this does not affect the noise generated by turbulence mixing [6].

Seeding particles are produced by a PIVTEC Pivpart45 generator, comprised by 45 Laskin nozzles and using Shell Ondina 919 oil, with average size of 1 μm. These particles have a relaxation time of 1 μs [23], which is suitable due to the flow acceleration in the nozzle. The illumination is provided by laser pulses generated with a double-cavity Quantel CFR200 Nd:YAG system. This equipment provides a laser wavelength of 532 nm, with a maximum energy of 200 mJ/pulse, and a pulse duration of 8 ns. Two LaVision Imager SX4M cameras (resolution: 2360 $\times$ 1776 pixel; frame rate: 31 Hz; pixel size: 5.5 $\times$ 5.5 μm; minimum time interval: 250 ns; digital output: 12 bit), positioned 0.5 m distant of the jet axis, are used for image recording. The cameras are equipped with two Nikkor f/1.8 lenses of 50 mm focal length. This configuration allows for measurements of two fields-of-view (FOV), in order to capture a larger portion of the jet development, as shown in Fig. 6a. The FOVs of each camera are shown in Fig. 6b with an overlap of $1.25D_j$ between them. The final FOV has a dimension of $12D_j \times 4D_j$ (0.6 m $\times$ 0.2 m), and it is shown by the black lines. The resolution in the final FOV is approximately 6 pixel/mm.

With this set-up, 1000 pairs of particle images are acquired with a sampling rate of 15 Hz. The illumination and image acquisition are triggered synchronously by the LaVision DaVis 8.4 software, which is also used for the post-processing of the images. The separation time between paired images is tuned with respect to the jet velocity in order to obtain a maximum of 25 pixels displacement at the jet core. This value is chosen to ensure a displacement of at least 3 pixels at regions of lower velocity. A multi-pass cross-correlation algorithm [24] with window deformation [25] is applied. The final interrogation window size is 24 $\times$ 24 pixel^2 with an overlap factor of 75%, which provides a final spatial resolution of 4 mm and a vector spacing of 1 mm. Spurious vectors, on the order of 1% of the total amount, are discarded by applying a universal outlier

Table 3
PIV set-up and acquisition parameters.

Parameter	Value
Cameras	2 x LaVision Imager SX4M
Acquisition frequency [Hz]	15
Max. pixel displacement [px]	25
Field-of-view 1-2 [mm]	400×310
Final field-of-view [mm]	600×200
Spatial scaling factor [px/mm]	6
Interrogation window [px^2]	24×24
Overlap factor [%]	75
Vectors per velocity field	600×200
Vector spacing [mm^2]	1×1

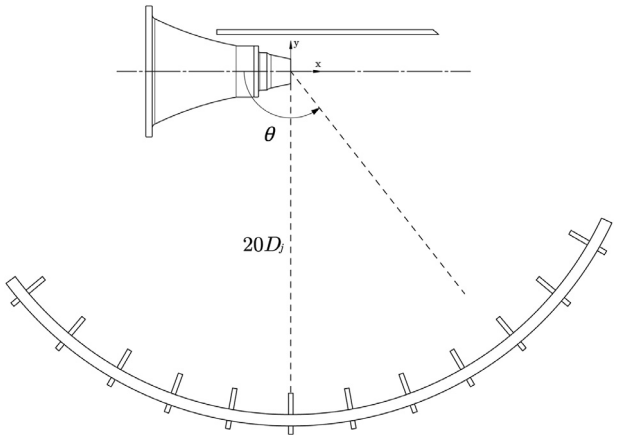

Fig. 7. Sketch of the microphone arc-array for far-field measurements. 12 microphones are placed from 40° to 150° ($\theta = 0°$ is upstream of the jet axis), spaced of 10°. The array is mounted at the reflected side of the plate for the installed configuration.

detector and are replaced by interpolation based on adjacent data [26]. The main parameters of the PIV set-up are reported in Table 3.

The estimation of the uncertainty in the PIV measurements is performed following the method proposed by Wieneke [27]. This method provides the uncertainty of a PIV displacement field by projecting the particles from one point to another with the obtained vectors and checking the resultant disparity [27]. The calculations result in a maximum uncertainty of $0.03U_j$ for the mean velocity, and $0.04u'_{rms}$ inside the potential core region. At the lipline ($y = 0.5D_j$), due to the strong flow unsteadiness, maximum uncertainty values of $0.06U_j$ and $0.08u'_{rms}$ are obtained.

2.3.2. Acoustic measurements

The acoustic measurements are carried out with 12 Bruel & Kjaer 4938 1/4" microphones (frequency range: 4 Hz to 70 kHz; pressure-field response: ±2 dB; max. output: 172 dB ref. 2×10^{-5} Pa). The microphones are integrated to Bruel & Kjaer 2670 - 1/4" microphone preamplifiers, and a Bruel & Kjaer NEXUS Type 2690-A conditioner is also used to amplify the recorded signals. The microphones are mounted on an arc-array dimensioned for measurements at 1 m radius ($20D_j$, centered at the origin of the coordinates system). The polar angle follows the convention of $\theta = 0°$ in the upstream direction of the jet axis. Therefore, the microphone at $\theta = 90°$ is aligned with the nozzle exit. The microphones are mounted from $\theta = 40°$ to $\theta = 150°$, spaced of 10°, as shown in Fig. 7.

For the installed configuration, the arc-array is mounted on the reflected side of the plate (jet in between the plate and array), in order to assess the effect of the flow-permeable materials on the reflection of jet acoustic waves as well. The measurements are performed with a sampling frequency of 51.2 kHz for 20 s. For post-processing, the acoustic data are split into blocks of 2048 samples for each Fourier transform, and windowed with a Hanning weighting function with 50% overlap. These parameters result in a frequency resolution of 25 Hz. The spectra shown in the following sections have been also scaled to an observer at a distance of $100D_j$ from the origin, similarly as performed in the JIN benchmark studies at NASA Glenn [2].

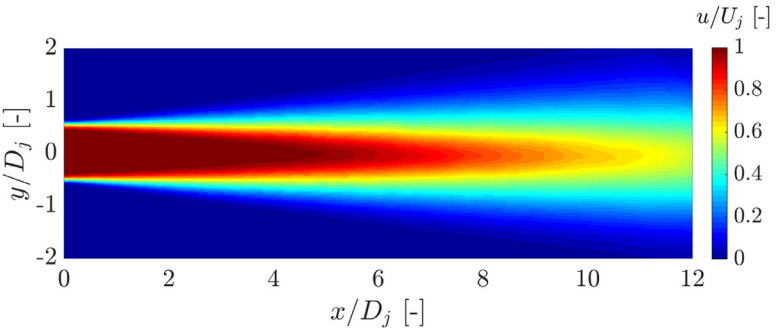

Fig. 8. Contour plot of the time-averaged jet axial velocity u for a $M_a = 0.5$ condition.

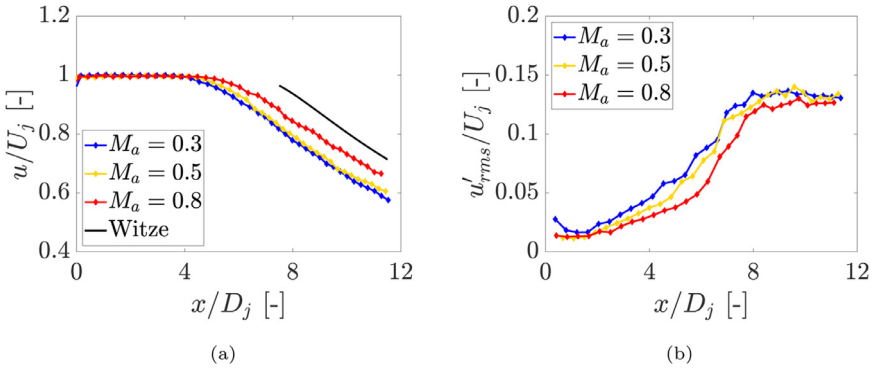

Fig. 9. Profiles of (a) time-averaged axial velocity and (b) r.m.s. of axial velocity fluctuations at the jet centerline for three jet velocities. The centerline velocity decay follows the trend defined by Witze [28].

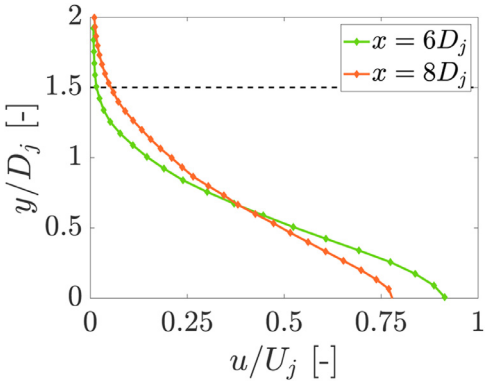

Fig. 10. Profiles of time-averaged axial velocity in the radial direction at three axial stations. The dashed line corresponds to the closest flat plate position, relative to the jet in the installed configurations.

3. Results and discussions

3.1. Jet flow field

In this section, the flow field of the isolated jet is discussed. The PIV measurements are performed for the 3 investigated acoustic Mach numbers and the results are displayed in terms of time-averaged axial velocity u and the r.m.s. of velocity fluctuations (u'_{rms}). The jet development for $M_a = 0.5$ is shown in the contour plot in Fig. 8. The region corresponding to the potential core and the downstream velocity decay can be detected, as well as the spreading of the jet and symmetry with respect to the centerline.

The velocity profiles are extracted at the jet centerline and plotted in Fig. 9. The quantities are non-dimensionalized by the respective jet nominal velocity U_j. The potential core length X_c, defined as the distance between the point where $u = 0.98U_j$ and the nozzle exit, is reported in Table 4 for all jet velocities. These values are compared with results obtained

Table 4
Potential core lengths obtained from experimental measurements (X_c) and Witze's equation (X_W) for three jet velocities.

M_a [-]	X_c/D_j [-]	X_W/D_j [-]
0.3	4.4	4.6
0.5	5.0	5.1
0.8	5.4	5.8

from Witze's equation for predicting the potential core length X_W of compressible free jets [19,28]:

$$\frac{X_W}{D_j} = \frac{4.375(\rho_j/\rho_\infty)^{0.28}}{1 - 0.16M_j}, \tag{3}$$

where ρ_j and ρ_∞ are the jet and ambient densities, respectively. A good agreement is obtained between the experimental and predicted results. The centerline velocity decay downstream of the potential core is also shown to follow the trend defined by Witze with the equation [28]:

$$\frac{u}{U_j} = 1 - e^{\alpha/(1-x/X_W)}, \tag{4}$$

where α is a constant equal to 1.43 [19].

The increase in potential core length with the jet velocity is related to the change in the size of the structures in the mixing-layer with the jet Reynolds number [28]. For $M_a = 0.8$, the structures are likely to be smaller and thus, the merge of the shear layer at the centerline occurs further downstream. This is also confirmed by the r.m.s. of velocity fluctuations, plotted in Fig. 9b, which are also lower for higher jet velocities.

Velocity profiles in the radial direction are also obtained at two axial stations, corresponding to the trailing-edge positions of the investigated installed jet configurations ($x = 6D_j$ and $x = 8D_j$). The profiles are plotted in Fig. 10, along with a line at $y = 1.5D_j$, which is the radial position where the plate is closest to the jet, for $M_a = 0.3$. Similar results have been obtained for the other jet velocities. It is shown that the axial velocity is zero at $y = 1.5D_j$ for $x = 6D_j$ and, therefore, a plate with a trailing edge at this position is located outside of the plume. Conversely, for $x = 8D_j$, at $y = 1.5D_j$, the local axial velocity is non-zero and equal to $0.05U_j$. However, due to the relatively low velocity at this point, it is not likely that the surface significantly changes the characteristics of the turbulent structures in the mixing-layer, i.e. no changes in the noise due to turbulence mixing are expected even for the longest surface. These results also allow for the calculation of the jet spreading angle δ. Values of $\delta = 9^\circ$ ($M_a = 0.3$); $\delta = 8.9$ ($M_a = 0.5$) and $\delta = 8.6$ ($M_a = 0.8$) are obtained. These results are consistent with those from the NASA Glenn tests [19], and they confirm that the jet is fully turbulent.

3.2. Far-field acoustic results

In this section, the results of the acoustic measurements for the installed jet with flow-permeable materials are reported and compared with the isolated and installed (solid trailing edge) jets, initially for the baseline plate configuration ($L = 6D_j$ and $h = 1.5D_j$). Two types of flow-permeable materials are investigated: a metal foam and a perforated plate with straight holes; both inserts have a length $L_p = 3D_j$. The results are displayed in Fig. 11 as Sound Pressure Level (SPL - ref. 2×10^{-5} Pa) versus Strouhal number St ($St = f \times D_j/U_j$), at three polar angles ($\theta = 40^\circ$, $\theta = 90^\circ$ and $\theta = 150^\circ$) and different jet velocities. The spectra have been plotted starting at a frequency of 350 Hz ($St = 0.18$ for $M_a = 0.3$), which is the minimum value for which the room has anechoic properties.

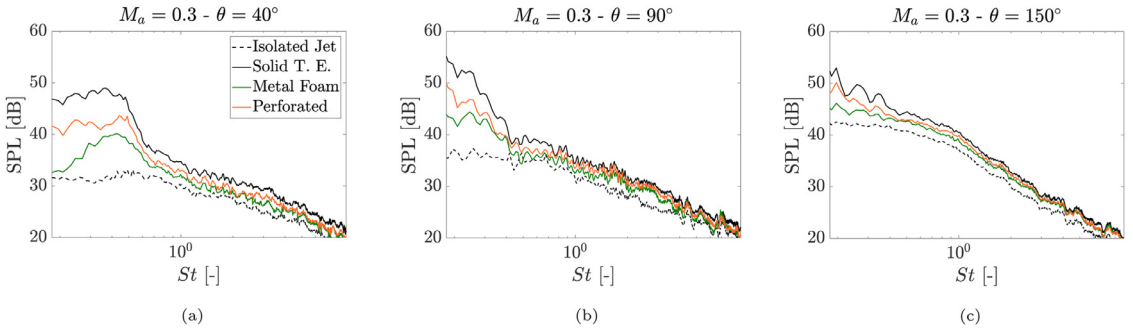

Fig. 11. Isolated and installed jet spectra, with solid and flow-permeable surfaces ($L_p = 3D_j$), at three polar angles ($\theta = 40^\circ$, $\theta = 90^\circ$ and $\theta = 150^\circ$) and three velocities. (a), (b) and (c) $M_a = 0.3$. (d), (e) and (f) $M_a = 0.5$. (g), (h) and (i) $M_a = 0.8$.

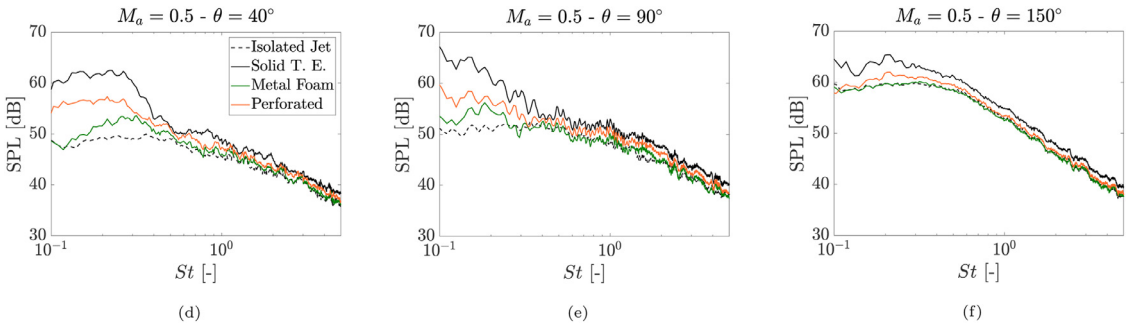

Fig. 11. Continued

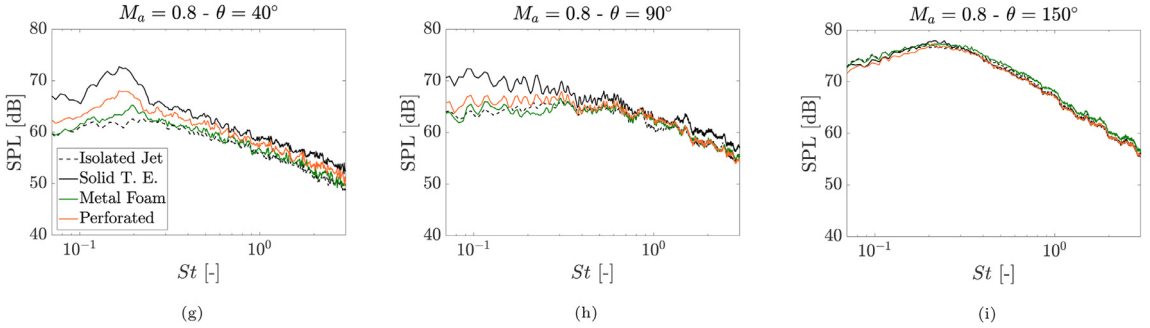

Fig. 11. Continued

Firstly, comparing the spectra for isolated and installed jets (solid plate), it is shown that installation effects are responsible for a strong noise increase at low and mid frequencies; for $M_a = 0.3$ and $\theta = 40°$, there is a 17 dB increase in SPL with respect to the isolated case at the installed spectral peak ($St = 0.37$). This strong noise amplification occurs up to $St = 0.7$ for this condition, and at higher frequencies there is a constant shift of approximately 3 dB from the isolated curve, which characterizes reflection of acoustic waves on the surface. In the sideline direction ($\theta = 90°$), the SPL increases for $St < 0.3$, whereas for $0.3 < St < 0.6$ there is a reduction with respect to the upstream direction. Therefore, for $\theta = 90°$, the spectral peak shifts to a lower frequency, possibly lower than the range where the measured data are reliable; this implies that the effect of the flow-permeable materials at the spectral peak might be not significant for a full-scale application, where the peak is likely located below the hearing range. Nonetheless, for a frequency of $St = 0.25$, there is also a 17 dB increase with respect to the isolated case. In the downstream direction of the jet ($\theta = 150°$), there is a maximum amplification of 7 dB at $St = 0.25$ due to the dipolar directivity of the noise generated by the plate, as well as increased noise from turbulence mixing by the jet. For higher jet velocities, similar trends are obtained, but the relative amplification with respect to the isolated noise levels is lower due to increased significance of turbulence-mixing noise.

For the plates with flow-permeable treatments, the spectra show considerable noise reduction with respect to the solid installed case, mainly at low and mid frequencies, where installation effects are dominant. For $M_a = 0.3$ and $\theta = 40°$, reductions of 9 dB and 7 dB are seen at the spectral peak ($St = 0.37$) for the metal foam and perforated inserts, respectively. The spectral amplitude is also reduced for $St > 0.7$, indicating that the flow-permeable materials, particularly the metal foam, reduce the effects of acoustic wave reflection on the surface. For $\theta = 90°$, despite the strong low-frequency noise increase, there is still a significant reduction with the permeable trailing edges; 9 dB and 6 dB for $St < 0.25$ with the metal foam and perforated, respectively. Finally, for $\theta = 150°$, 5 dB and 3 dB reductions occur at $St = 0.25$. Moreover, since the installation effects are weak in this direction, the noise levels with the flow-permeable trailing edges are similar to those of the isolated jet.

Comparing the two different treatments, the metal foam provides more benefits than the perforated inserts for all tested cases. Since the former has a higher permeability, it is likely that the differences in noise levels between the two cases can be attributed to a better pressure balance between the upper and lower sides of the plate for the metal foam case, thus reducing the surface pressure fluctuations near the trailing edge and, consequently, the noise due to scattering. The differences between the two flow-permeable configurations is more noticeable at low frequencies ($St < 0.4$). This occurs because, for $\theta = 40°$, while the noise reduction with the perforated trailing edge is approximately constant for $St < 0.5$, for the metal foam there is a change in the spectral shape, with a new distinct peak at $St = 0.45$, in that direction. This is an indication that there is an additional noise source other than the trailing edge.

Similar trends are obtained for higher jet velocities. For $M_a = 0.5$, there is a similar absolute noise abatement at the spectral peak as the previous case (10 dB reduction with the metal foam and 6 dB with the perforated). For this velocity, the

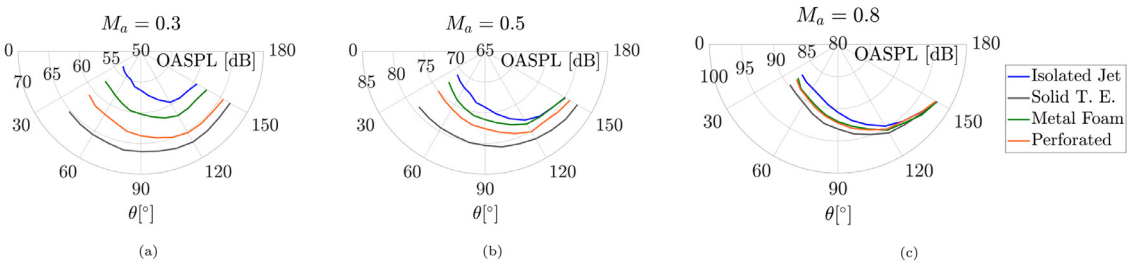

Fig. 12. Directivity plots of Overall Sound Pressure Level (OASPL) of isolated and installed jets with solid and flow-permeable surfaces ($L_p = 3D_j$), for three jet velocities.

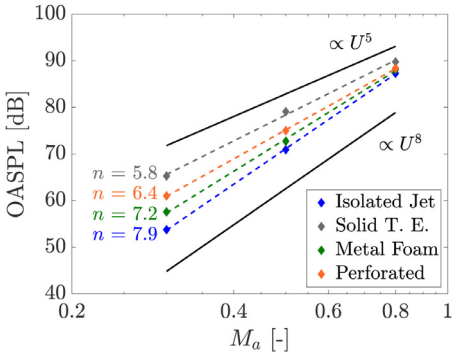

Fig. 13. Scaling of Overall Sound Pressure Level with the jet acoustic Mach number for isolated and installed configurations, with solid and flow-permeable trailing edges.

Table 5
Difference in OASPL between solid and flow-permeable (metal foam and perforated) installed cases for a polar angle $\theta = 40^\circ$ and three jet velocities. The overall increases due to installation effects with respect to isolated levels are also included as reference.

M_a [-]	ΔOASPL$_{SLD-ISO}$ [dB]	ΔOASPL$_{SLD-MF}$ [dB]	ΔOASPL$_{SLD-PERF}$ [dB]
0.3	11.5	7.7	4.3
0.5	8.2	6.4	4.1
0.8	2.5	1.7	1.4

noise increase due to installation effects is relatively lower when compared to the $M_a = 0.3$ jet. Therefore, with the same absolute noise reduction provided by the flow-permeable materials, the spectra approach more the levels of the isolated configuration. This effects becomes more visible for the $M_a = 0.8$ jet, where the curves of both treated surfaces practically collapse with the isolated one for $\theta > 90^\circ$, indicating that the trailing-edge source has been completely mitigated in these cases.

The Overall Sound Pressure Level (OASPL) for each case is calculated at all polar angles by integrating the SPL spectra in the range of 350 Hz $< f <$ 20 kHz and the results are shown in the polar plots in Fig. 12, for three jet velocities.

The directivity plots show that the highest differences between isolated and installed (solid plate) cases are found in the upstream direction, which is consistent with noise from scattering at the plate trailing edge [4]. In the downstream direction, this difference is smaller and the installed curves tend to collapse with the ones of the isolated jet, especially for the highest jet velocity. The results also show that the flow-permeable materials are effective in reducing jet-installation noise in all assessed directions, particularly upstream. This indicates that the dipole sources on the plate are mitigated. In the downstream direction, for the metal foam case, the levels reach those of the isolated jet for $\theta > 120^\circ$ and $M_a > 0.5$, indicating that there is no change in the turbulence-mixing noise component due to the presence of the plate.

The differences between the OASPL for flow-permeable and solid surfaces are reported in Table 5, for a polar angle $\theta = 40^\circ$. The overall increase due to installation effects with respect to the isolated jet is also included for reference. It can be seen that the metal foam provides higher noise reduction than the perforated structure, particularly for $M_a = 0.3$. From the 11.5 dB overall increase due to installation effects, it is possible to reduce 7.7 dB by applying the metal foam at the plate trailing edge. For higher jet velocities, the installation noise is practically eliminated with this porous material. Despite having a lower permeability, the perforated trailing edge still provides significant noise reduction, of approximately 4 dB for $M_a = 0.3$ and $M_a = 0.5$.

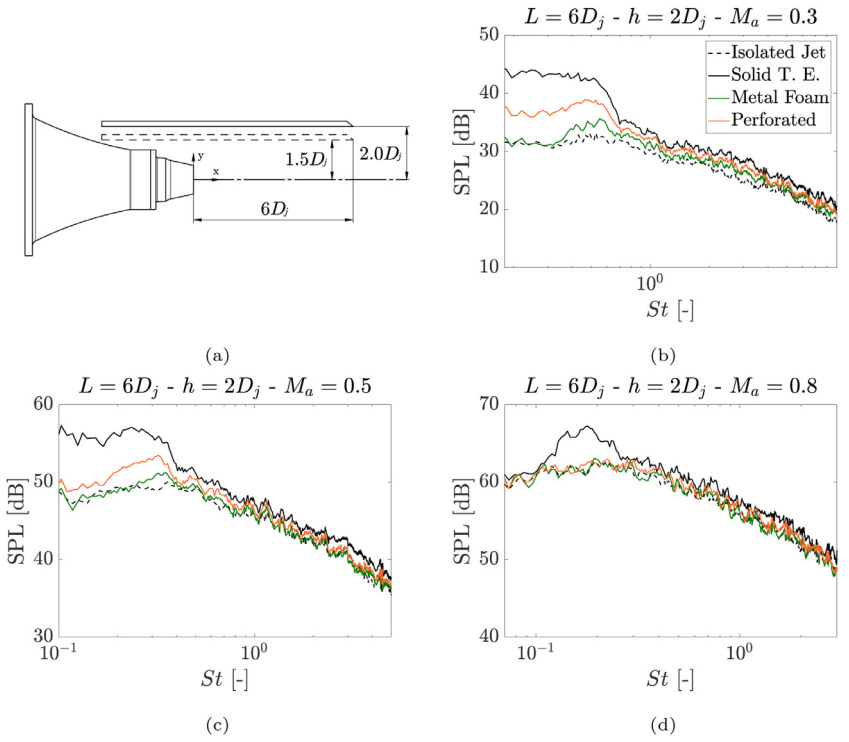

Fig. 14. Isolated and installed jet spectra, with solid and flow-permeable surfaces ($L_p = 3D_j$), obtained for a plate with $L = 6D_j$ and $h = 2.0D_j$ (effect of surface height) at a polar angle $\theta = 40^\circ$ and three velocities.

The dependence of the OASPL with the jet velocity for an angle $\theta = 40^\circ$ is also calculated and plotted in Fig. 13 for each case. Reference curves are also added for OASPL $\propto U_j^8$, which is consistent for turbulence-mixing noise [29], and OASPL $\propto U_j^5$, consistent with scattering at the surface trailing edge [3]. By applying the permeable treatment, the exponent of noise levels with the jet velocity increases from $n = 5.8$ to $n = 6.4$, for the perforated plate, and to $n = 7.2$ for the metal foam. The isolated jet has $n = 7.9$. These results are in qualitative agreement with those from Geyer and Sarradj [13]. This confirms that, when flow-permeable treatments are applied to the surface, the scattering becomes less dominant with respect to other sources such as turbulence-mixing.

The effect of the configuration geometry on the noise reduction that can be achieved using flow-permeable materials is investigated in the following. Firstly, the effect of the plate radial position is addressed by moving the plate in this direction. The spectra shown in Fig. 14 are obtained for a plate with $L = 6D_j$ and $h = 2.0D_j$ at a polar angle $\theta = 40^\circ$. This configuration is shown in Fig. 14a with solid lines; the dashed lines correspond to the baseline case ($L = 6D_j$ and $h = 1.5D_j$). The results show that at this height and for $M_a = 0.3$, for example, noise reductions up to 10 dB and 6 dB with respect to the solid case are achieved for the metal foam and perforated plate, respectively, for $St = 0.37$. These values are similar to those obtained for the previous case with the plate closer to the jet ($h = 1.5D_j$). For the metal foam trailing edge, the noise levels collapse with those of the isolated configuration for $M_a = 0.5$ and higher. The perforated insert also provides significant noise reduction; there is still a trailing-edge noise component at low frequencies for $M_a = 0.5$ (up to 4 dB with respect to the isolated levels), but at $M_a = 0.8$ the installation effects are also not visible for this configuration.

Since lower absolute levels are obtained in the spectra for the treated plate farther from the jet, it is interesting to plot the results in terms of noise reductions with respect to each solid case. The curves in Fig. 15 are given in terms of ΔSPL for the respective plate height, and for each permeable configuration, for $M_a = 0.3$. Higher jet velocities are not shown since the turbulence-mixing noise becomes significant and it is not possible to properly assess the effect of the permeable materials. It can be seen that the curves are similar, with minor local deviations, indicating that the absolute noise reductions provided by the permeable materials are independent on the plate radial position, i.e. independent on the amplitude of impinging pressure waves. It is likely that this property is also the reason why the SPL for the installed jets with flow-permeable trailing-edges approach more the isolated jet levels for higher jet velocities.

The effect of the plate length is investigated for a surface with $L = 8D_j$ and $h = 1.5D_j$, as shown in Fig. 16 for $\theta = 40^\circ$. The results show that, for this geometry, there is a significant noise increase at low frequencies ($St < 0.35$, for $M_a = 0.3$). Moreover, the benefits provided by the flow-permeable materials are lower than in the previous cases (6 dB decrease at $St = 0.35$, for $M_a = 0.3$ and both types of inserts). At mid frequencies ($0.35 < St < 0.7$, for $M_a = 0.3$), the metal foam and perforated inserts provide similar noise reduction for this configuration. The main differences between the two of them

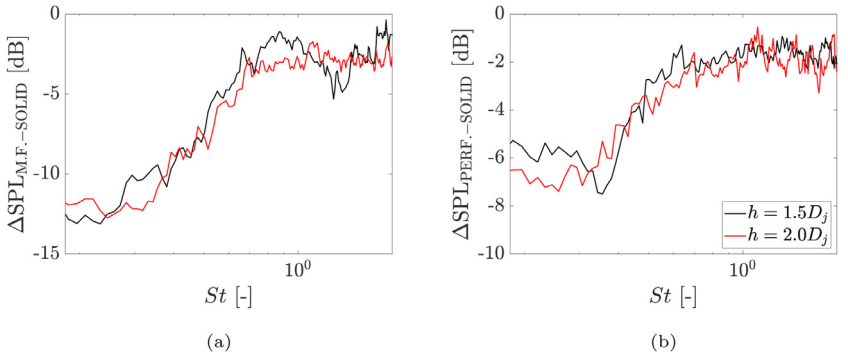

Fig. 15. Reduction in noise levels with respect to the solid case for each plate height, obtained at $\theta = 40^\circ$ and for $M_a = 0.3$. (a) Metal foam. (b) Perforated.

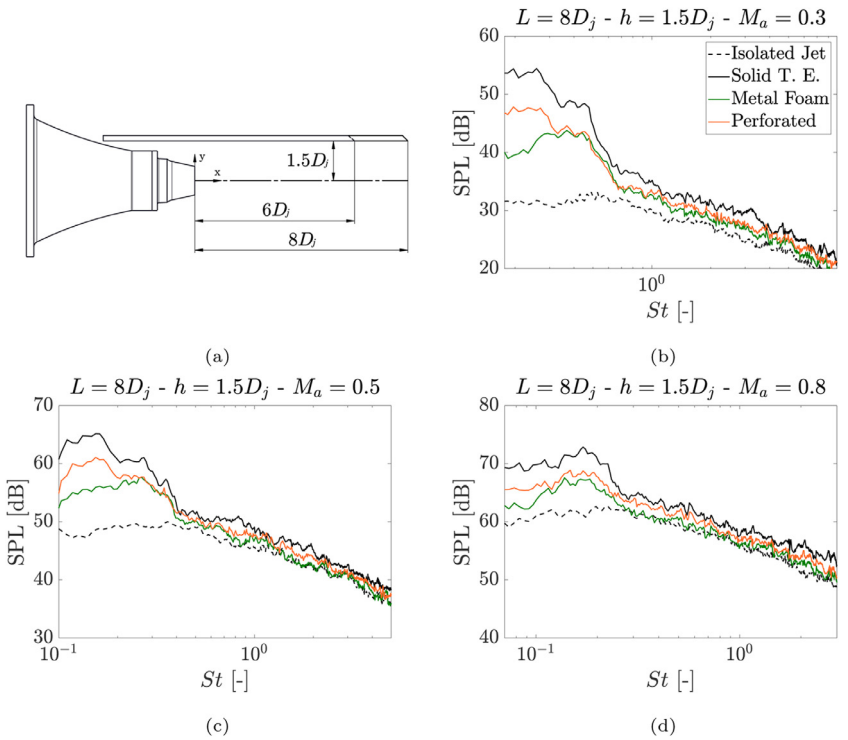

Fig. 16. Isolated and installed jet spectra, with solid and flow-permeable surfaces ($L_p = 3D_j$), obtained for a plate with $L = 8D_j$ and $h = 1.5D_j$ (effect of plate length) at a polar angle $\theta = 40^\circ$ and three velocities.

occur in the range of noise increase due to the increment in the plate length. This is likely the result of the different permeability of the surfaces at the trailing edge, where large-scale pressure waves impinge on the plate; the metal foam provides a better pressure balance between the upper and lower sides of the plate, thus better reducing the surface pressure fluctuations at low frequencies. On the other hand, it is likely that the noise at $0.35 < St < 0.7$ is generated by surface fluctuations upstream of the flow-permeable region, which is the same for both cases. Similar trends occur for the other jet velocities.

This effect can be verified by analysing the influence of the flow-permeable insert length on the noise reduction, for a fixed plate length $L = 6D_j$ and height $h = 1.5D_j$. Measurements are taken for inserts with length $L_p = 1D_j$, and compared to the ones previously shown ($L_p = 3D_j$). Spectra are plotted in Fig. 17, for a polar angle $\theta = 40^\circ$ and three M_a. The results show that, for the metal foam, the smaller insert still provides significant noise abatement, particularly for $M_a = 0.3$ (6 dB reduction at the peak). For $M_a = 0.5$, similar absolute noise reductions are obtained and, for $M_a = 0.8$, the curves are more similar since turbulence-mixing noise is significant. Therefore, longer flow-permeable sections provide higher benefits since there is a shorter solid section of the plate subjected to strong surface pressure fluctuations. For the perforated structure, the small insert ($L_p = 1D_j$) provides less noise reduction, of approximately 4 dB at $St = 0.37$, for $M_a = 0.3$. The difference in amplitudes between the curves for the two insert lengths is also more significant at low frequencies ($St < 0.3$ for $M_a = 0.3$),

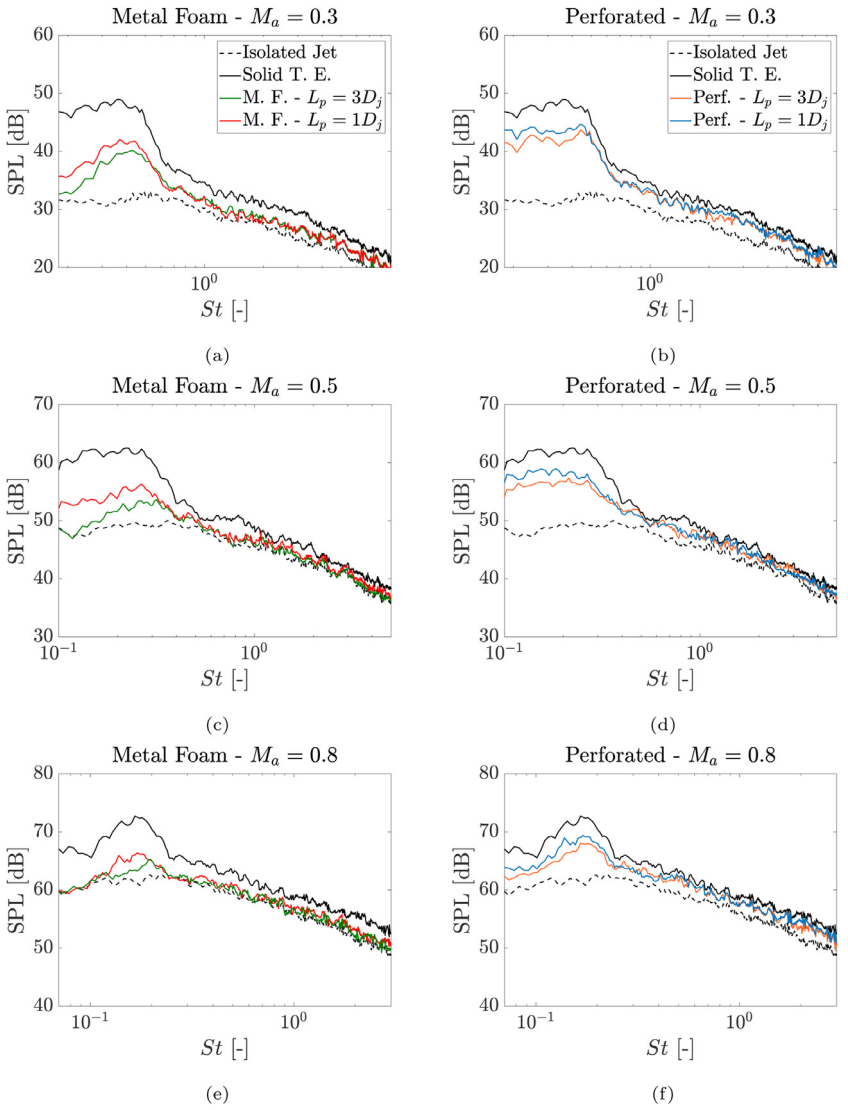

Fig. 17. Isolated and installed jet spectra, with solid and flow-permeable surfaces ($L_p = 3D_j$ and $L_p = 1D_j$ - effect of porosity length), for a plate with $L = 6D_j$ and $h = 1.5D_j$, at a polar angle $\theta = 40^\circ$ and three velocities.

indicating that the additional solid length, for the cases with a shorter insert, generates noise in this frequency range. This is a similar behaviour to that of increasing the overall plate length, as shown in Fig. 16. Nonetheless, it can be concluded that even small sections of permeable treatment are sufficient for achieving noise reduction. This is important since those types of structures usually lead to performance degradation (loss of lift and drag increase) [12,16].

It is shown that the solid extension of the plate affects the final spectral shape and amplitude, also shifting the frequency of peak SPL. Therefore, it is also important to analyze the effect of changing the length of the porous insert, but keeping the size of the solid section of the plate constant. For that purpose, spectra of two cases are compared: $L = 6D_j$ with $L_p = 1D_j$ and $L = 8D_j$ with $L_p = 3D_j$. Therefore, both cases have a solid section of $5D_j$ between the nozzle exit and the flow-permeable section. Results are shown in Fig. 18, for the two types of permeable materials and three M_a. The results are similar to those shown in Fig. 17. The case with an overall longer plate has more noise generated at lower frequencies ($St < 0.3$ for $M_a = 0.3$), for both metal foam and perforated inserts; at $St = 0.27$, there is a 5 dB difference between the metal foam curves and 4.4 dB for the perforated ones. Therefore, this is likely attributed to the difference in total plate length so that the noise is generated due to the impingement of high-amplitude and low-frequency pressure waves on the flow-permeable region of the plate. On the other hand, the noise at mid frequencies does not show significant change when comparing the two cases. Therefore, it is probable that the dominant source in this range is the same for both of them, and it is likely that the source is now located at the solid-permeable junction in the plate.

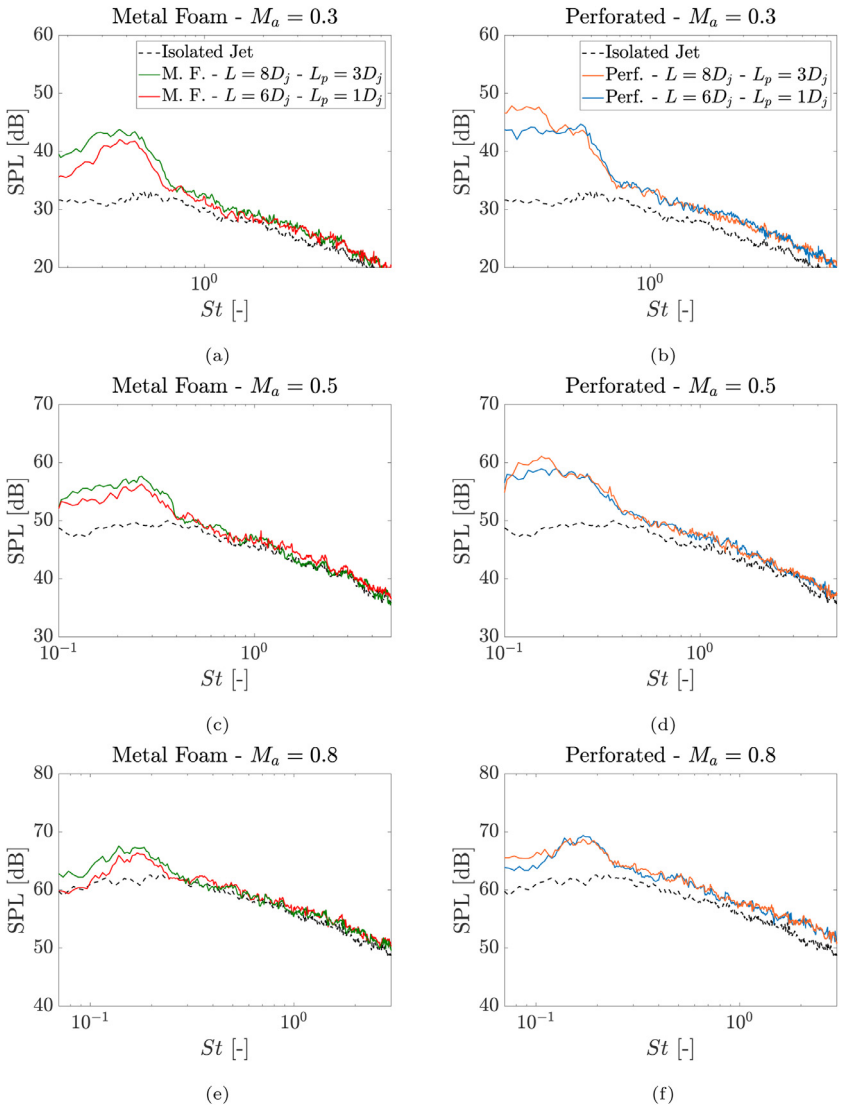

Fig. 18. Isolated and installed jet spectra, with flow-permeable inserts and same solid length ($L = 8D_j$ with $L_p = 3D_j$ and $L = 6D_j$ with $L_p = 1D_j$), at a polar angle $\theta = 40^\circ$ and three velocities.

It is speculated that the junction between solid and flow-permeable surfaces has become the dominant source location for the metal foam case. The effect of the junction has been described in the literature as an additional geometric singularity, and thus, as a new scattering region, as shown by Kisil and Ayton [30]. Scattering at the junction is then responsible for noise increase at mid and high frequencies, also changing the directivity pattern of the overall configuration [30]. Moreover, beamforming results from Rubio-Carpio et al. [16] showed that, for frequencies where TBL-TE noise reduction is achieved with flow-permeable materials, the dominant source is placed at the solid-flow-permeable junction [16]. Therefore, it is possible that there is an additional contribution from that region, particularly for the cases with the metal foam due to its high permeability. The junction effect would thus be the cause of the different spectral shape, as well as of the SPL peak at a higher frequency, relative to the fully solid and perforated cases. The results previously shown for the metal foam case are in agreement with this hypothesis; for the reduced insert length, the junction is placed at $x = 5D_j$ (as opposed to $x = 3D_j$ in the baseline case), and the spectral peak shifts towards a lower frequency (Fig. 17). On the other hand, when the junction is placed at the same position and the porous extent is changed, there is simply an increase in amplitude, but the spectral peak frequency remains unchanged (Fig. 18). This effect is likely not obtained with the perforated configuration, since the low permeability does not result in a strong impedance jump at the junction, and, consequently, scattering at that region. Further work is necessary to confirm these hypotheses.

4. Conclusions

An experimental study on the effect of flow-permeable materials on the noise produced by an installed jet is performed. The configuration is comprised by a single-stream subsonic jet and a nearby flat plate, placed in the jet near-field. Two types of flow-permeable structures are investigated: a metal foam and a perforated insert with straight holes normal to the axis. The metal foam has a higher porosity and permeability than the perforated structure and its channels are also interconnected.

Planar PIV measurements are carried out to characterize the jet velocity field. Based on the potential core length and spreading angle, it is concluded that the jet has a turbulent behaviour for all tested velocities. Moreover, it is confirmed that there is no direct grazing of the jet on the plate, except for the longest surface tested. However, for this case, the surface is in a region of very low velocities compared to the potential core, and it is likely not affecting the noise generated by turbulence mixing. Acoustic measurements show that the installation effects are responsible for strong low-frequency noise increase with respect to isolated levels. This amplification is more significant at a low jet velocity, where the dipole sources on the surface are more acoustically efficient than the quadrupole sources from turbulent mixing. The spectral shape and amplitude are shown to be dependent on the geometry of the configuration; longer surfaces produce more noise at low frequencies, whereas moving the plate towards the jet in the radial direction results in noise increase, especially at mid frequencies.

Significant noise reduction is achieved when the solid plate trailing edge is replaced by flow-permeable inserts, particularly in the low/mid frequency range, where the scattering is the dominant mechanism. Comparing the two types of structures, the metal foam is more effective in reducing JIN, likely due to a higher permeability, which can mitigate the pressure imbalance between the upper and lower sides of the plate, and thus reduce the noise generated by surface pressure fluctuations. For low jet velocities, a noise decrease of up to 10 dB is obtained at the spectral peak with the metal foam, but the installation noise is still visible. When the jet velocity is increased, the attenuation provided by the flow-permeable treatment brings the noise levels closer to the isolated case, and the trailing-edge source is no longer dominant with respect to the jet quadrupoles. It is worth mentioning that the highest noise levels for the investigated installed configurations occur at low frequencies ($St < 0.3$ for $M_a = 0.3$), particularly at the sideline direction ($\theta = 90^\circ$). For a full-scale aircraft, these frequencies may not be of particular significance. However, the flow-permeable trailing edges assessed in this work also provide noise reductions at mid and high frequencies, including reflection effects on the surface, which would be significant in a full-scale configuration.

The effect of surface treatment is also assessed for different configuration geometries. By moving the plate away from the jet, flow-permeable materials provide similar absolute noise reduction as the baseline case. Conversely, by increasing the plate length, lower noise abatement is obtained with the flow-permeable treatments, particularly at low frequencies ($St < 0.35$ for $M_a = 0.3$), with the metal foam still providing higher benefits. On the other hand, the noise at mid frequencies ($0.35 < St < 0.7$ for $M_a = 0.3$) is similar for the two types of insert, indicating that it is generated by the impingement of pressure waves in the solid region of the plate, upstream of the flow-permeable treatments.

For a fixed plate length, a shorter flow-permeable insert is shown to provide noise reductions with respect to the solid case, but in a lower degree compared to the larger insert. The main differences occur at low frequencies, which indicates that the increased noise is due to the additional solid length, compared to the case with the longer insert. The frequency of highest SPL also shifts towards low frequencies. On the other hand, when the plate length is changed, but the solid-permeable junction is kept at the same axial position, the flow-permeable materials behave differently. For the metal foam, there is an increase in amplitude, but no significant change to the spectral peak frequency, whereas for the perforated there is a low-frequency noise increase with a change in the spectral peak. It is believed that this difference is caused by the high permeability of the metal foam, which produces a new singularity and thus a new scattering region at the solid-permeable junction.

These results show that a surface treatment with flow-permeable materials is a potentially promising mitigation solution for jet-installation noise. However, the mechanisms that provide such reductions are still unclear. Further work is required to investigate the phenomena happening at the junction region and inside the flow-permeable structure, particularly focusing on the change of impedance, pressure imbalance and the effect of permeability/resistivity of the flow-permeable structures, since it is possible to achieve substantial noise reduction with a perforated structure, even with a low porosity.

Declaration of Competing Interest

The authors declare that they have no known competing financial interests or personal relationships that could have appeared to influence the work reported in this paper.

CRediT authorship contribution statement

Leandro Rego: Conceptualization, Methodology, Validation, Formal analysis, Investigation, Data curation, Writing - original draft, Writing - review & editing, Visualization. **Daniele Ragni:** Investigation, Writing - review & editing, Visualization, Resources, Supervision, Project administration, Funding acquisition. **Francesco Avallone:** Writing - review & editing, Visualization, Supervision. **Damiano Casalino:** Writing - review & editing, Visualization, Supervision. **Riccardo Zamponi:** Inves-

tigation, Writing - review & editing, Visualization, Resources, Supervision. **Christophe Schram:** Writing - review & editing, Resources, Supervision.

Acknowledgements

This work is part of the IPER-MAN project (Innovative PERmeable Materials for Airfoil Noise Reduction), project number 15452, funded by the Netherlands Organization for Scientific Research (NWO). The authors would like to thank Alejandro Rubio-Carpio, for providing the parameters from the flow-permeable materials characterization. The authors would also like to thank Dr. Mirjam Snellen and Prof. Sybrand van der Zwaag from the Delft University of Technology, for collaboration in the project.

References

[1] J.L.T. Lawrence, M. Azarpeyvand, R.H. Self, Interaction between a flat plate and a circular subsonic jet, in: 17th AIAA/CEAS Aeroacoustics Conference, Portland, OR, USA, 2011, doi:10.2514/6.2011-2745.
[2] C. Brown, Jet-surface interaction test: far-field noise results, in: Proceedings of the ASME Turbo Expo 2012: Power for Land, Sea and Air, Copenhagen, Denmark, 2012, pp. 1–13.
[3] J.E. Ffowcs-Williams, L.H. Hall, Aerodynamic sound generation by turbulent flow in the vicinity of a scattering half plane, J. Fluid Mech. 40 (4) (1970) 657–670, doi:10.1017/S0022112070000368.
[4] R.W. Head, M.J. Fisher, Jet/surface interaction noise: - analysis of farfield low frequency augmentations of jet noise due to the presence of a solid shield, in: 3rd AIAA Aeroacoustics Conference, Palo Alto, CA, USA, 1976, doi:10.2514/6.1976-502.
[5] I. Belyaev, G. Faranosov, N. Ostrikov, G. Paranin, A parametric experimental study of jet-flap interaction noise for a realistic small-scale swept wing model, in: 21st AIAA/CEAS Aeroacoustics Conference, Dallas, TX, USA, 2015, doi:10.2514/6.2015-2690.
[6] L. Rego, F. Avallone, D. Ragni, D. Casalino, Noise amplification effects due to jet-surface interaction, AIAA Scitech 2019 Forum, San Diego, CA, USA, 2019, doi:10.2514/6.2019-0001.
[7] A.V.G. Cavalieri, P. Jordan, W.R. Wolf, Y. Gervais, Scattering of wavepackets by a flat plate in the vicinity of a turbulent jet, J. Sound Vibr. 333 (24) (2014) 6516–6531, doi:10.1016/j.jsv.2014.07.029.
[8] D. Casalino, A. Hazir, Lattice Boltzmann based aeroacoustic simulation of turbofan noise installation effects, in: 23rd International Congress on Sound & Vibration, Athens, Greece, 2014, pp. 1–8.
[9] C. Hughes, The promise and challenges of ultra high bypass ratio engine technology and integration, AIAA Aerospace Sciences Meeting, Orlando, FL, USA, 2011.
[10] V.G. Mengle, L. Brusniak, R. Elkoby, R.H. Thomas, Reducing propulsion airframe aeroacoustic interactions with uniquely tailored chevrons: 3. Jet-flap interaction, in: 12th AIAA/CEAS Aeroacoustics Conference, Cambridge, MA, USA, 2006, doi:10.2514/6.2006-2435.
[11] J.D. Revell, H.L. Kuntz, F.J. Balena, B.L. Storms, R.P. Dougherty, Trailing-edge flap noise reduction by porous acoustic treatment, in: 3rd AIAA/CEAS Aeroacoustics Conference, Atlanta, GA, USA, 1997, doi:10.2514/6.1997-1646.
[12] E. Sarradj, T. Geyer, Noise generation by porous airfoils, in: 13th AIAA/CEAS Aeroacoustics Conference, Rome, Italy, 2007, doi:10.2514/6.2007-3719.
[13] T. Geyer, E. Sarradj, Trailing edge noise of partially porous airfoils, in: 20th AIAA/CEAS Aeroacoustics Conference, Atlanta, GA, USA, 2014, doi:10.2514/6.2014-3039.
[14] M. Herr, K. Rossignol, J. Delfs, N. Lippitz, M. Mößner, Specification of porous materials for low-noise trailing-edge applications, in: 20th AIAA/CEAS Aeroacoustics Conference, Atlanta, GA, USA, 2014, doi:10.2514/6.2014-3041.
[15] A. Rubio Carpio, R. Merino Martínez, F. Avallone, D. Ragni, M. Snellen, S. Van Der Zwaag, Broadband trailing edge noise reduction using permeable metal foams, in: InterNoise Conference, Hong Kong, 2017.
[16] A. Rubio Carpio, R. Merino Martínez, F. Avallone, D. Ragni, M. Snellen, S. Van Der Zwaag, Experimental characterization of the turbulent boundary layer over a porous trailing edge for noise abatement, J. Sound Vibr. 443 (2019) 537–558, doi:10.1016/j.jsv.2018.12.010.
[17] D. Guariglia, A. Rubio-Carpio, C. Schram, Design of a facility for studying shock-cell noise on single and coaxial jets, Aerospace 5 (1) (2018) 25, doi:10.3390/aerospace5010025.
[18] C. Brown, J. Bridges, Small Hot Jet Acoustic Rig Validation, Technical Report, NASA/TM-2001-214234, Cleveland, OH, USA, 2006.
[19] J. Bridges, M. Wernet, Establishing consensus turbulence statistics for hot subsonic jets, in: 16th AIAA/CEAS Aeroacoustics Conference, Stockholm, Sweden, 2010, pp. 1–41, doi:10.2514/6.2010-3751.
[20] S. Kim, C. Lee, A review on manufacturing and application of open-cell metal foam, Procedia Mater. Sci. 4 (2014) 305–309, doi:10.1016/j.mspro.2014.07.562.
[21] Tenco DDM, DLP Digital Light Processing Data Sheet, URL http://tenco-online.com/wp-content/uploads/2017/03/Datasheets-Tenco-DDM.pdf.
[22] D.B. Ingham, I. Pop, Transport Phenomena in Porous Media, first ed., Pergamon, Kidlington, Oxford, UK, 1998, doi:10.1016/B978-0-08-042843-7.X5000-4.
[23] D. Ragni, F. Schrijer, B.W. Van Oudheusden, F. Scarano, Particle tracer response across shocks measured by PIV, Exp. Fluids 50 (1) (2011) 53–64, doi:10.1007/s00348-010-0892-2.
[24] F. Scarano, M.L. Riethmuller, Advances in iterative multigrid PIV image processing, Exp. Fluids 29 (7) (2000) S051–S060, doi:10.1007/s003480070007.
[25] F. Scarano, Iterative image deformation methods in PIV, Meas. Sci. Technol. 13 (1) (2001).
[26] J. Westerweel, F. Scarano, Universal outlier detection for PIV data, Exp. Fluids 39 (6) (2005) 1096–1100, doi:10.1007/s00348-005-0016-6.
[27] B. Wieneke, PIV uncertainty quantification from correlation statistics, Meas. Sci. Technol. 26 (7) (2015), doi:10.1088/0957-0233/26/7/074002.
[28] P.O. Witze, Centerline velocity decay of compressible free jets, AIAA J. 12 (4) (1974) 417–418, doi:10.2514/3.49262.
[29] M.J. Lighthill, On sound generated aerodynamically I. General theory, Proc. R. Soc. A (1952) 564–587, doi:10.1098/rspa.1952.0060.
[30] A. Kisil, L.J. Ayton, Aerodynamic noise from rigid trailing edges with finite porous extensions, J. Fluid Mech. 836 (2018) 117–144, doi:10.1017/jfm.2017.782.